

Object-fabrication Targeted Attack for Object Detection

Xuchong Zhang[†], Changfeng Sun[†], Haoliang Han, Hang Wang, Hongbin Sun*, *Senior Member, IEEE* and Nanning Zheng, *Fellow, IEEE*

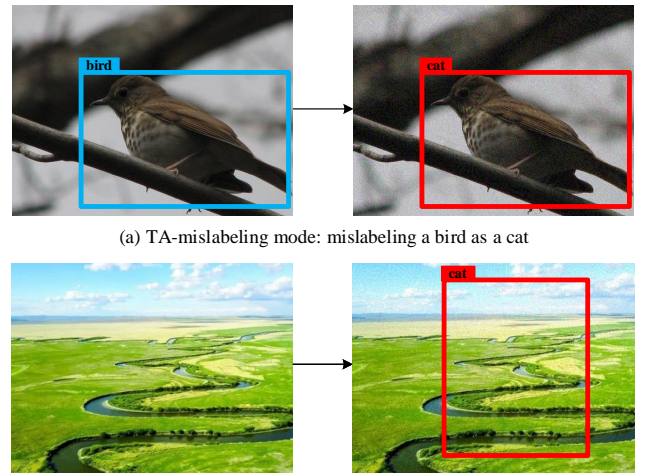
Abstract—Recent researches show that the deep learning based object detection is vulnerable to adversarial examples. Generally, the adversarial attack for object detection contains targeted attack and untargeted attack. According to our detailed investigations, the research on the former is relatively fewer than the latter and all the existing methods for the targeted attack follow the same mode, i.e., the object-mislabeled mode that misleads detectors to mislabel the detected object as a specific wrong label. However, this mode has limited attack success rate, universal and generalization performances. In this paper, we propose a new object-fabrication targeted attack mode which can mislead detectors to ‘fabricate’ extra false objects with specific target labels. Furthermore, we design a dual attention based targeted feature space attack method to implement the proposed targeted attack mode. The attack performances of the proposed mode and method are evaluated on MS COCO and BDD100K datasets using FasterRCNN and YOLOv5. Evaluation results demonstrate that, the proposed object-fabrication targeted attack mode and the corresponding targeted feature space attack method show significant improvements in terms of image-specific attack, universal performance and generalization capability, compared with the previous targeted attack for object detection. Code will be made available.

Index Terms—Targeted attack, object detection, adversarial examples, dual attention.

I. INTRODUCTION

Object detection [1] is one of the most fundamental tasks in computer vision community and tremendous progress has been achieved by employing deep neural networks. Due to the excellent performance of object detection, it has been applied to many applications including autonomous driving [2], [3], intelligent surveillance [4], [5], mobile robot [6], [7], etc. However, a variety of researches [8]–[11] have shown that the detection network is vulnerable to adversarial attack and gives wrong predictions when encountering adversarial examples crafted by adding human-imperceptible perturbations to input images. The study of attack methods not only helps to reveal the reasons for the vulnerability of the detection network, but also helps to improve the robustness of the detection model.

Generally, the adversarial attacks for object detection can be grouped into untargeted attacks and targeted attacks. The former aims to mislead the detectors to predict objects to other



(a) TA-mislabeled mode: mislabeling a bird as a cat

(b) TA-fabrication mode: fabricating a cat on an image even without detected objects

Fig. 1. The illustrations of the TA-mislabeled and the TA-fabrication mode.

arbitrary labels or none labels [12], [13], while the latter is used to fool the detectors to predict certain specific wrong labels [14], [15]. Recent researches have unfolded three modes for the untargeted attack: (1) object-vanishing mode that removes the detectors’ ability in recognizing any objects [16]–[18]; (2) object-mislabeled mode that misleads detectors to mislabel existing objects as arbitrary wrong labels [19], [20]; (3) object-fabrication mode that misleads detectors to predict extra false objects with arbitrary labels [21], [22]. Compared with the untargeted attack, the targeted attack is a more challenging task since it attempts to predict specific labels rather than arbitrary labels. Therefore, there are relatively few methods [14], [15] designed for the targeted attack and they all follow the same mode, i.e., the object-mislabeled targeted attack mode (abbreviated to TA-mislabeled). As shown in Fig. 1(a), TA-mislabeled aims to fool detectors to mislabel an existing object in the source image as a specific wrong label. According to our analyses and the following experiments, this mode shows low attack success rate, poor universal performance, and weak generalization capability. Hence, designing a more efficient targeted attack mode is a practically interesting and challenging task.

In this paper, we propose a new targeted attack mode for object detection, namely object-fabrication targeted attack (abbreviated to TA-fabrication). As shown in Fig. 1(b), TA-fabrication aims to mislead detectors to detect extra false objects with specific target labels. The visible difference between TA-mislabeled and TA-fabrication is whether the

[†] Equal contribution.

X Zhang, C Sun, H Han, H Sun and N Zheng are with the College of Artificial Intelligence, Xi’an Jiaotong University, Xi’an 710049, P.R. China

H Wang is with the College of Microelectronics, Xi’an Jiaotong University, Xi’an 710049, P.R. China

* Corresponding author: Hongbin Sun, hsun@mail.xjtu.edu.cn

targeted attack relies on an existing object that has already been detected in the source image. Compared with the TA-mislabeled mode, the proposed TA-fabrication mode may have the following three advantages.

- *High attack success rate.* The TA-mislabeled usually fails in the situations that no object to be attacked in the source image and large gap between the correct label and the specified wrong label of the attacked object. In contrast, the TA-fabrication has a high attack success rate because this mode aims to ‘fabricate’ an extra specific object to deceive detectors and can be conducted on the source images even without similar object or any detected object.
- *Fine universal performance.* The same object may have totally different scales, colors, positions and features in different images. Therefore, it is difficult for TA-mislabeled to generate a universal perturbation that misleads detectors to mislabel the same object in different images as another wrong label. The adversarial example generated by TA-fabrication is independent of the objects detected in the images, thus it is easier to design a universal perturbation to mislead detectors to predict a preassigned object in different images.
- *Strong generalization capability.* Poor universal performance generally implies weak generalization capability. Because the adversarial examples generated by TA-mislabeled mode are highly related to the detected objects in the source image, the adversarial perturbations are usually invalid for unseen data. In contrast, TA-fabrication may be easily generalized to new images because of its fine universal performance.

As mentioned above, previous works [14], [15], [19], [20] design various methods to achieve the TA-mislabeled attack, and the generic approach is to attack the classification score of the detected objects in order to change their original labels. Thus, these methods cannot be directly exploited to achieve the TA-fabrication attack. To mislead the detectors to predict extra target objects out of nothing, we further propose a targeted feature space attack (TFA) method to implement the proposed TA-fabrication mode for object detection. Firstly, we introduce a guided image which contains the target objects to generate adversarial examples by driving the extracted features of source images towards the target object’s features extracted from the guided image. Then, we design a dual attention mechanism to efficiently filter out the critical features of the target object in the whole feature space. Specifically, the spatial attention is used to determine the spatial location of the target object, and the class attention is used to select the most critical channels that are associated with the semantic information of the target object. By optimizing a loss function consisting of two feature spaces, the semantic features of the target object can be transferred to the source image and the adversarial example for the TA-fabrication mode is obtained. In order to evaluate the proposed TFA method and TA-fabrication mode, we conduct extensive experiments on MS COCO and BDD100K datasets to attack two representative object detection models, i.e. FasterRCNN [23] and

YOLOv5 [24]. Because the existing methods are inappropriate to achieve the TA-fabrication attack, we implement a variant of the previous method [20] to compare the performance with TFA. The experimental results clearly demonstrate that the proposed TFA method and the proposed TA-fabrication mode achieve significant improvements in the cases of the image-specific attack success rates, universal performance and generalization capability.

II. RELATED WORK

The adversarial example [25]–[29] was originally proposed to disrupt an image classifier by adding a small perturbation which is imperceptible by human to the input images. Then, the researches of the adversarial example were extended to other tasks [30]–[35] and gradually evolved into two types of methods, i.e. untargeted attack and targeted attack. This paper mainly focuses on the targeted attack for object detection.

The goal of the targeted attack is to fool the detectors to detect a specific wrong label. Based on our extensive investigations, the researches on targeted attack are relatively fewer than untargeted attack. Xie *et.al.* [19] propose the first targeted method named dense adversary generation (DAG), which assigns a specific adversarial label to the proposals, then designs a loss function to maximize the classification score of that label and finally performs iterative gradient backpropagation to purposely mislabel the proposals. Based on DAG, Nezami *et.al.* [15] attack a designated object in an image and preserve the labels of other detected objects in the image by adding large perturbations to the bounding box of the designated object. Chow *et.al.* [20] propose a targeted adversarial objectness gradient attack (TOG). By adding human-imperceptible perturbations to source images, TOG attempts to improve the classification score of a specific class and reduce the classification score of an initially detected object, thus achieving object-mislabeled attack. Based on TOG, Cai *et.al.* [14] introduce joint training strategy and context information to mislabel detected objects as the specific wrong labels and enhance the transferability of the adversarial examples. In these methods, [19] and [15] are designed for attacking only two-stage detectors, while TOG is appropriate for both one-stage and two-stage detectors. Besides, TOG also achieves remarkable targeted attack performance.

We can see that all the existing targeted attack methods for object detection follow the same mode, i.e., TA-mislabeled. The detection network is usually updated by optimizing the loss function consisting of bounding boxes regression, objectness measures and class probability vectors. All the previous works attack the final output layer to achieve the TA-mislabeled by maximizing the detected object’s classification score of the specific wrong label. Therefore, these methods cannot be directly applied to the TA-fabrication mode since it needs to fool detectors to firstly predict an extra object and then maximize the classification score of that object. This motivates us to further design an efficient method to achieve the proposed TA-fabrication attack.

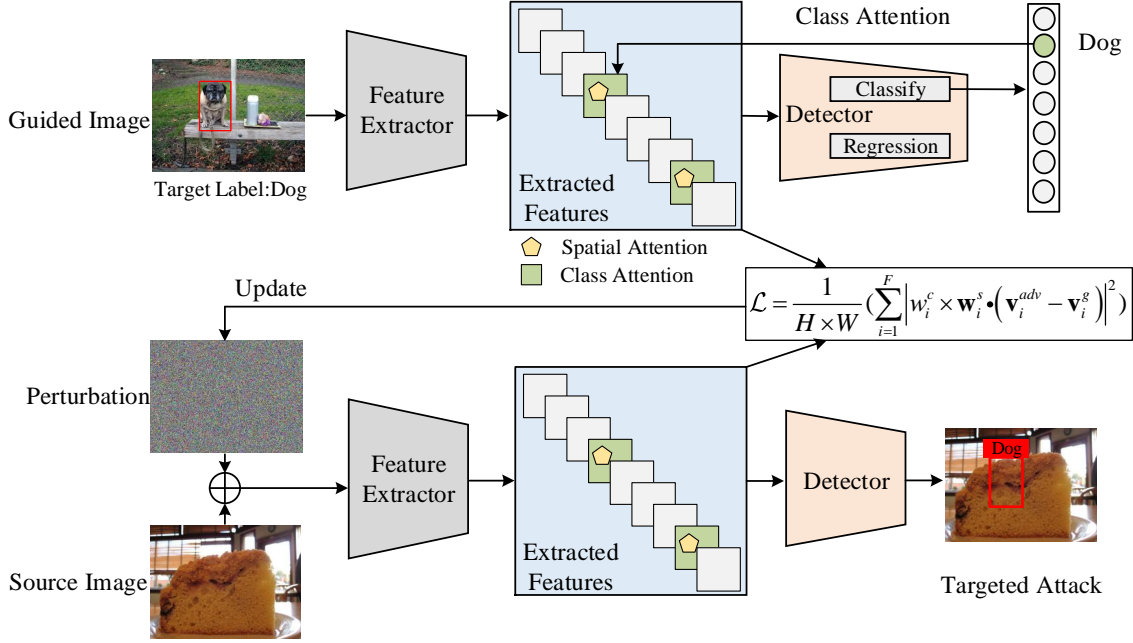


Fig. 2. The framework of the proposed targeted feature space attack. A source image \mathbf{x}^s and a guided image \mathbf{x}^g containing a target object o^t are used to conduct the targeted attack. Firstly, the features of the guided image and adversarial example are extracted by two identical detection models, i.e. \mathbf{v}_i^g and \mathbf{v}_i^{adv} . Then, the critical features that represent o^t are filtered out by the proposed dual attention mechanism. Finally, the adversarial example can be obtained by optimizing a loss function \mathcal{L} consisting of the attention weights (w_i^c , w_i^s) and features (\mathbf{v}_i^g , \mathbf{v}_i^{adv}).

III. METHOD

A. Overall Framework

In order to ‘fabricate’ a fake object in the source image without relying on the detected object, a guided image containing the target object is introduced specifically to achieve the TA-fabrication attack. Moreover, we propose to attack the internal feature layer of the detection model instead of the final output layer which exploited in the traditional TA-mislabeling attack. The key idea of the proposed method is to employ the targeted feature space attack to change part of the semantic feature of the source image towards that of the target object in the guided image, thus fooling the detector to predict the target object with a specific label in the source image.

The overall framework of the proposed TFA is shown in Fig. 2. Firstly, a well-trained object detection model is applied to extract the features of the guided image and the source image. Then, a dual attention mechanism is employed to filter out the critical features that can represent the target object (e.g. dog) in the extracted features of the guided image. Next, the small perturbation is constantly updated by optimizing the loss function consisting of the guided image feature space and adversarial example feature space. Eventually, the final adversarial example for the specific class can be obtained by adding the perturbation to the source image. In the following content, we will formulate the proposed targeted attack mode and present the attack process in detail.

B. TFA Formulation

Given an input source image \mathbf{x}^s , an object detector G without suffering from any attacks is able to correctly detect the objects \mathbf{O}^s that are originally contained in the image, i.e. $G(\mathbf{x}^s) = \mathbf{O}^s$, where \mathbf{O}^s is a small subset of the whole object

dataset $\{o_1, o_2, o_3, \dots, o_n\}$. The goal of the proposed targeted attack mode is to find adversarial examples $\mathbf{x}^{adv} = \mathbf{x}^s + \delta$ such that $G(\mathbf{x}^{adv})$ can yield a new target object o^t ($o^t \notin \mathbf{O}^s$) on a certain region of \mathbf{x}^s . δ is an imperceptible perturbation which should be limited to a small range. In this paper, we use the ℓ_∞ norm to restrict the value of δ less than ϵ , i.e., $\|\delta\|_\infty \leq \epsilon$. Therefore, the optimization of \mathbf{x}^{adv} for the targeted attack is formulated as,

$$\mathbf{x}^{adv} = \arg \min_{\mathbf{x}} \mathcal{L}(G(\mathbf{x}), o^t), s.t. \|\mathbf{x}^{adv} - \mathbf{x}^s\|_\infty \leq \epsilon, \quad (1)$$

where $\mathcal{L}(G(\mathbf{x}), o^t)$ is the loss function constructed by the feature spaces of the guided image and adversarial example. It is calculated as,

$$\mathcal{L} = \frac{1}{H \times W} \left(\sum_{i=1}^F |\mathbf{w}_i \cdot (\mathbf{v}_i^{adv} - \mathbf{v}_i^g)|^2 \right), \quad (2)$$

where \mathbf{v}_i^{adv} denotes the i -th channel of the extracted features of the adversarial example \mathbf{x}^{adv} , \mathbf{v}_i^g denotes the i -th channel of the extracted features of the guided image \mathbf{x}^g , F is the total number of the feature channels, H and W are the horizontal and vertical resolutions of the feature map, \mathbf{w}_i is the attention weight to differentiate the importance of different features and more specific descriptions are presented in the next subsection. Based on Equation (1) and (2), we can conclude that the adversarial example is optimized by gradually driving the corresponding features of the source image towards the critical features of the target object in the guided image.

C. Class Attention and Spatial Attention

As mentioned above, filtering out the key features of the target object in the whole feature space is critical to achieve the proposed targeted attack. Hence, we propose a dual attention

mechanism to address this problem, which includes a class attention and a spatial attention.

The class attention is used to select the most critical channels in the extracted features which are closely associated with the semantic information of the target object. Inspired by [36], we use the derivative of the objectness with respect to the extracted features \mathbf{v}^g to indicate the contribution of different channels to the category classification of the target object, thus these different contributions can be calculated and regarded as the class attention weight \mathbf{w}^c . Specifically, it is formulated as the global-average-pooling over the width and height dimensions.

$$\hat{w}_i^c = \frac{1}{H \times W} \sum_m \sum_n \frac{\partial y^t}{\partial \mathbf{v}_{imn}^g}, \quad (3)$$

where y^t is the confidence score of the specific class t , \hat{w}_i^c is the class weight of the i -th channel, and i, m, n in \mathbf{v}_{imn}^g are the indices of the feature channel, width and height dimensions respectively. It should be noted that, \hat{w}_i^c has positive and negative values, where the former means the i -th feature channel has positive correlation with the class of the target object, and the latter means the i -th feature channel has negative correlation with the class of the target object. We only keep the positive values, thus the final class attention weight w_i^c is calculated as,

$$w_i^c = \max(\hat{w}_i^c, 0) = \max\left(\frac{1}{H \times W} \sum_m \sum_n \frac{\partial y^t}{\partial \mathbf{v}_{imn}^g}, 0\right). \quad (4)$$

A large value of w_i^c means that the i -th channel is more relevant to the semantic feature of the target object.

The spatial attention is used to determine the spatial location of the target object in feature space. As shown in [37], the activation values at the locations containing objects are usually much larger than those containing the background in the feature map. Therefore, we define the positive values of the feature map \mathbf{v}_i^g as the spatial attention weight,

$$\mathbf{w}_i^s = \max(\mathbf{v}_i^g, 0). \quad (5)$$

A large value in \mathbf{w}_i^s means that the corresponding position has a high probability of being an object than background.

After obtaining the class attention weight and the spatial attention weight, the final dual attention weight is defined as,

$$\mathbf{w}_i = w_i^c \times \mathbf{w}_i^s. \quad (6)$$

We need to point out that the proposed method is fundamentally different from the previous dual attention network (DANet) for scene segmentation [38]. DANet is proposed to model the semantic interdependencies in spatial and channel dimensions during training process in order to further improve the feature representation which contributes to more precise segmentation results. In comparison, the proposed dual attention is employed to select and locate the most critical features in the well-trained model which are closely related to the semantic representation of the target object. These two methods have different formulations and purposes.

Algorithm 1 Generating image-specific perturbation for object detection.

Input: source image \mathbf{x}^s , guided image \mathbf{x}^g , object detector G , restriction ϵ , step size α
Output: adversarial example \mathbf{x}^{adv}
 $\mathbf{v}^g \leftarrow G(\mathbf{x}^g)$
 Compute class attention \mathbf{w}^c using Equation (4)
 Compute spatial attention \mathbf{w}^s using Equation (5)
 Compute dual attention \mathbf{w} using Equation (6)
 $\mathbf{x}^{adv} \leftarrow \mathbf{x}^s$
for $t \leftarrow 0$ **to** max_{iter} **do**
 $\mathbf{v}_t^{adv} \leftarrow G(\mathbf{x}^{adv})$
 compute loss \mathcal{L} using Equation (7)
 $\delta_t \leftarrow Clip\left(\delta_{t-1} - \alpha \times sign\left(\frac{\partial \mathcal{L}}{\partial \delta_{t-1}}\right), -\epsilon, \epsilon\right)$
 $\mathbf{x}_t^{adv} \leftarrow Clip(\mathbf{x}_{t-1}^{adv} + \delta_t, 0, 255)$.
return \mathbf{x}_t^{adv}

Algorithm 2 Generating universal perturbation for object detection.

Input: source image set \mathcal{X}^s , guided image \mathbf{x}^g , object detector G , restriction ϵ , step size α
Output: adversarial examples set \mathcal{X}^{adv} , universal perturbation δ
 $\mathbf{v}^g \leftarrow G(\mathbf{x}^g)$
 Compute class attention \mathbf{w}^c using Equation (4)
 Compute spatial attention \mathbf{w}^s using Equation (5)
 Compute dual attention \mathbf{w} using Equation (6)
 $\mathbf{x}^{adv} \leftarrow \mathbf{x}^s$
 Initialize universal perturbation δ_0
for $t \leftarrow 0$ **to** max_{iter} **do**
for \mathbf{x}^s in \mathcal{X}^s **do**
 $\mathbf{x}_t^{adv} \leftarrow Clip(\mathbf{x}^s + \delta_{t-1}, 0, 255)$
 $\mathbf{v}_t^{adv} \leftarrow G(\mathbf{x}_t^{adv})$
 compute loss \mathcal{L} using Equation (7)
 $\delta_t \leftarrow Clip\left(\delta_{t-1} - \alpha \times sign\left(\frac{\partial \mathcal{L}}{\partial \delta_{t-1}}\right), -\epsilon, \epsilon\right)$
for \mathbf{x}^s in \mathcal{X}^s **do**
 \mathcal{X}^{adv} append $Clip(\mathbf{x}^s + \delta_t, 0, 255)$
return $\mathcal{X}^{adv}, \delta_t$

D. Attack Algorithm

According to Equation (2)–(6), the final loss function of the proposed targeted attack is presented as,

$$\mathcal{L} = \frac{1}{H \times W} \left(\sum_{i=1}^F |w_i^c \times \mathbf{w}_i^s \cdot (\mathbf{v}_i^{adv} - \mathbf{v}_i^g)|^2 \right). \quad (7)$$

It is necessary to reiterate that \mathbf{v}^{adv} is the extracted features of the adversarial example, i.e. $(\mathbf{x}^s + \delta)$. Then, we use an iterative way to minimize the above function and the adversarial perturbation of TFA is updated as follows.

$$\delta_t = Clip\left(\delta_{t-1} - \alpha \times sign\left(\frac{\partial \mathcal{L}}{\partial \delta_{t-1}}\right), -\epsilon, \epsilon\right), \quad (8)$$

where α is a fixed step size during optimization, $sign(\cdot)$ is the sign function, the function $Clip(\delta, -\epsilon, \epsilon)$ is used to restrict the value of δ to the range of $(-\epsilon, \epsilon)$. After a number of training iterations, the adversarial example related to the targeted object can be generated as,

$$\mathbf{x}^{adv} = Clip(\mathbf{x}^s + \delta, 0, 255). \quad (9)$$

Similar to [39], the proposed TFA algorithm can be used to generate both image-specific perturbation and universal (image-agnostic) perturbation. The image-specific perturbation [40] is generated on a certain image and can only attack this image, while the universal perturbation [41], [42] is generated on a image set and can attack most images of this set. The detailed generation processes are shown in Algorithm 1 and Algorithm 2, respectively.

IV. EXPERIMENTAL RESULTS

As introduced in the above sections, we firstly propose a new TA-fabrication attack mode for object detection, and then design a corresponding targeted feature space attack method since the previous approaches are not suitable for the TA-fabrication attack. In this section, we carry out extensive experiments to demonstrate the effectiveness of the proposed TFA method and TA-fabrication mode. Specifically, the following contents mainly contain the experimental comparisons of three aspects. (1) Subsection IV-B—TFA and a modified TOG for the TA-fabrication mode are evaluated in the cases of image specific attack performance, universal attack performance and generalization performance. (2) Subsection IV-C—We analyze the impacts of the perturbation degree, dual attention module and guided image on the performance of TFA individually. (3) Subsection IV-D—The comparative experiments between the TA-mislabeling mode and the TA-fabrication mode are conducted in the cases of success rate, universal performance and generalization capability.

A. Experimental Settings

1) *Dataset and Metric*: The experiments in this paper are conducted on MS COCO dataset [43] and BDD100K dataset [44]. MS COCO dataset is a large-scale dataset for multiple computer vision tasks. For object detection, MS COCO has the annotations of bounding boxes with 80 object categories. We randomly select 1000 samples as the source images and 8 target objects in different classes to conduct the targeted attack experiments. For each class, we randomly choose one sample which contains the corresponding target object as the guided image. In addition to MS COCO dataset, we also evaluate the proposed attack method on BDD100K dataset. BDD100K is a large-scale diverse driving dataset which has the annotations of bounding boxes with 10 object categories. Similarly, we randomly select 1000 samples as the source images and 6 target objects in different classes. For each class, we also choose one sample which contains the corresponding target object as the guided image. Fig. 3 shows part of the guided images containing the target objects.

Following [14], we use the success rate (SR) to evaluate the performance of attack methods. It is defined as the percentage

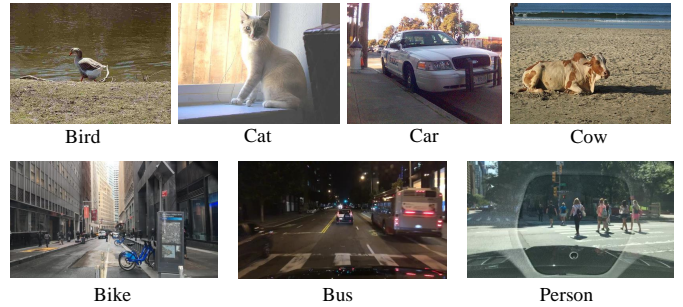


Fig. 3. Part of the guided images containing the target objects. First row is the guided images on MS COCO dataset, second row is the guided images on BDD100K dataset.

of successful attacks that the adversarial example obtained after training can precisely mislead the detector to predict the target object. Concretely, SR is calculated as,

$$SR = \frac{\text{Number of success attacks}}{\text{Number of all attacks}}. \quad (10)$$

During the experiments, each sample of the 1000 source images will be attacked with the 8 selected target objects for MS COCO dataset and 6 target objects for BDD100K dataset individually, thus we present SR for each class in the following results.

2) *Object Detectors*: In order to evaluate the attack performance on different object detectors, we exploit FasterRCNN and YOLOv5 to conduct the attack experiments, since they are the most representative detectors for two-stage detectors and one-stage detectors respectively. To ensure the detectors are well-trained, we use the default parameters released in official version^{1 2}. The confidence threshold for all detectors to output the detection results is set to 0.5.

3) *Comparison Methods*: As introduced in Section II, all the existing targeted attack methods attack the final output layers to achieve the TA-mislabeling mode and cannot be directly applied to the TA-fabrication mode. To make a comprehensive comparison, we modify the representative method TOG to implement the TA-fabrication attack. Specifically, the original TOG maximizes the classification score of the specific wrong label to mislabel one detected object, while we modify it to optimize the objectness score and classification score of the final output layer simultaneously in order to ‘fabricate’ designated target object. In the following contents, the original TOG for the TA-mislabel attack and the modified TOG for the TA-fabrication attack are denoted as TOG-M and TOG-F, respectively. TOG-F is used to evaluate the performance compared with the proposed TFA method and TOG-M is used to compare the performance between the proposed TA-fabrication mode and TA-mislabeling mode.

4) *Hyperparameter Settings*: The proposed framework involves a few hyperparameters, they are configured with same values for all methods. Specifically, the restriction value of the adversarial perturbation ϵ is set to 16, the number of iterations

¹<https://github.com/pytorch/vision>

²<https://github.com/ultralytics/yolov5>

TABLE I
THE IMAGE-SPECIFIC ATTACK PERFORMANCE COMPARISONS BETWEEN THE PROPOSED TFA AND TOG-F ON MS COCO DATASET.

Detector	Method	bird	cat	car	cow	dog	laptop	motor	teddy	average
FasterRCNN	TOG-F	17.9	29.3	22.6	6.8	26.6	13.6	6.5	13.9	17.2
	TFA	40.4	55.7	35.9	27.2	46.3	50.4	48.7	32.3	42.1
YOLOv5	TOG-F	0.4	0.1	0.0	0.0	0.8	0.0	0.0	0.1	0.2
	TFA	99.8	98.4	99.9	100.0	100.0	100.0	100.0	99.9	99.8

TABLE II
THE IMAGE-SPECIFIC ATTACK PERFORMANCE COMPARISONS BETWEEN THE PROPOSED TFA AND TOG-F ON BDD100K DATASET.

Detector	Method	bike	bus	motor	person	rider	truck	average
FasterRCNN	TOG-F	55.7	74.0	56.0	55.3	46.9	77.2	60.9
	TFA	99.6	98.1	90.5	86.1	72.1	96.5	90.5
YOLOv5	TOG-F	0.0	0.2	0.0	0.1	0.0	0.6	0.15
	TFA	100.0	98.8	99.6	100.0	91.5	99.9	98.3

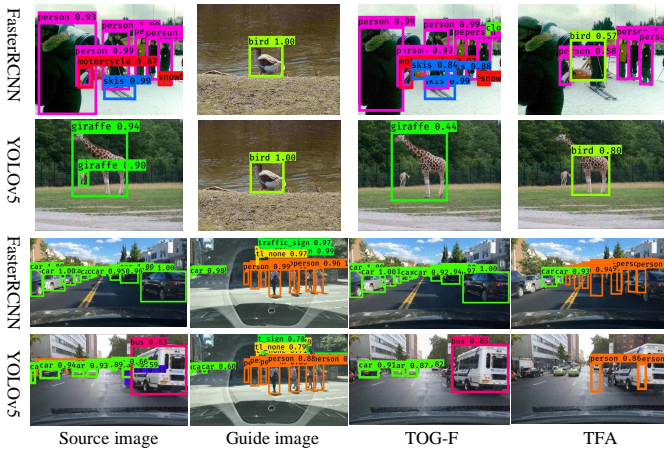


Fig. 4. The subjective illustrations of the proposed TFA and TOG-F on FasterRCNN and YOLOv5. The first two rows are the detection results of MS COCO dataset while the last two rows are the detection results of BDD100K dataset. Better to zoom in electronic version for viewing.

for one adversarial example is set to 80, and the step size α is set to 1.

B. TFA vs. TOG-F for TA-fabrication Mode

1) *Image-specific Attack Performance*: The image-specific adversarial examples are generated by Algorithm 1 and the attack success rate of each specific class is shown in Table I and Table II. We can see that the proposed TFA achieves significant improvements than TOG-F in terms of the success rate for all the target objects. Concretely, on MS COCO dataset, the average success rate of TFA are 42.1 and 99.8 for attacking FasterRCNN and YOLOv5, while the average success rate of TOG-F is only 17.2 and 0.2, respectively. On BDD100K dataset, TFA achieves 90.5 and 98.3 average success rate for attacking FasterRCNN and YOLOv5 while TOG-F only achieves 60.9 and 0.2, respectively. These results clearly demonstrate the effectiveness of our proposed TFA attack method.

An interesting phenomenon shown in Table I and II is that TOG-F seems to be more specialised in attacking FasterRCNN while TFA is more specialised in attacking YOLOv5. On MS

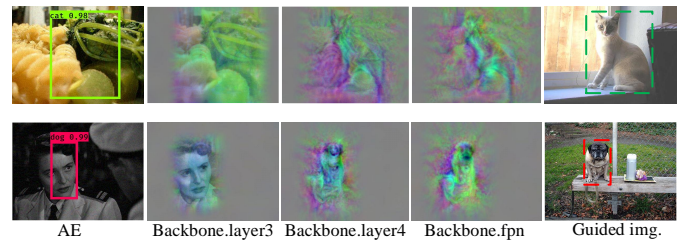


Fig. 5. The semantic information changes of different layers of FasterRCNN when performing TFA on two source images.

COCO and BDD100K datasets, the success rates of TOG-F on YOLOv5 are close to zero while the success rates of TOG-F for FasterRCNN are 17.2 and 60.9 respectively. As mentioned above, TOG-F attacks the final output layer to achieve the TA-fabrication mode by maximizing the classification score and objectness score. For the one-stage detector YOLOv5, the classification and objectness are calculated in the same output layer. We argue that the optimization directions of these two components may be inconsistent, thus leading to a non-convergence results and low success rate. In contrast, the two-stage detector FasterRCNN outputs the classification and objectness in different output layers, and they can be attacked and optimized separately to generate adversarial examples. For the proposed TFA, the success rates of YOLOv5 are higher than that of FasterRCNN on both datasets. We conjecture that this is mainly because the features extracted by YOLOv5 are more vulnerable to adversarial attack than that of FasterRCNN. The following experiments with respect to the perturbation degree in Fig. 8 also show that the features extracted by YOLOv5 can be easily changed by TFA even with small ϵ .

Fig. 4 further illustrates the subjective detection results of the proposed TFA and TOG-F on FasterRCNN and YOLOv5. The first column is the detections of the source images without any perturbations. The second column is the detections of the guided images containing the target objects (e.g. bird and person). The third and fourth columns are the detections of the adversarial examples generated by TOG-F and our TFA. Obviously, TOG-F fails to detect the targeted objects in these samples, and TFA can mislead the detectors to incorrectly

TABLE III
THE UNIVERSAL ATTACK PERFORMANCE COMPARISONS BETWEEN TOG-F AND THE PROPOSED TFA ON MS COCO DATASET.

Detector	Method	bird	cat	car	cow	dog	laptop	motor	teddy	average
FasterRCNN	TOG-F	32.0	18.3	50.0	32.0	13.9	10.0	14.8	20.5	23.9
	TFA	44.3	55.1	57.2	25.8	40.1	49.9	25.0	35.3	41.6
YOLOv5	TOG-F	0.3	1.1	0.1	0.0	0.0	0.0	0.0	0.1	0.2
	TFA	88.1	77.8	91.7	88.1	84.4	88.0	81.9	80.3	85.0

TABLE IV
THE UNIVERSAL ATTACK PERFORMANCE COMPARISONS BETWEEN TOG-F AND THE PROPOSED TFA ON BDD100K DATASET.

Detector	Method	bike	bus	motor	person	rider	truck	average
FasterRCNN	TOG-F	65.4	80.7	60.4	72.3	53.3	73.3	67.6
	TFA	97.3	85.6	83.0	99.8	75.5	90.0	88.5
YOLOv5	TOG-F	0.0	1.0	0.3	0.1	0.0	2.6	0.7
	TFA	99.4	95.5	97.6	100.0	88.6	96.4	96.3

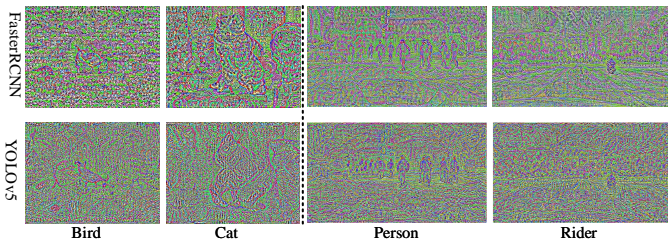


Fig. 6. The visualization results of the universal perturbations for the target objects bird, cat, person and rider. The first two columns are generated on MS COCO dataset while the last two columns are generated on BDD100K dataset.

detect the specified class at a certain image region where there is not even any object.

Fig. 5 illustrates the semantic information changes of different layers of FasterRCNN when performing TFA on two source images. By employing the feature inversion technique [45], we can see that as the layers progress from shallow to deep, the semantic features of the target objects (e.g., cat and dog) are gradually transferred to the feature maps of the source images. This demonstrates that the feature space is vulnerable to perturbations and can be changed purposely.

2) *Universal Attack Performance*: The universal perturbations and the corresponding adversarial examples are generated by Algorithm 2, and the universal attack results of TOG-F and TFA on two datasets are shown in Table III and Table IV. As it can be observed, the attack success rates of TFA are much higher than that of TOG-F for each specific class. This demonstrates that an elaborate targeted feature space attack has a better universal performance than the method attacking the final output layer for the TA-fabrication mode. Similar to the image-specific attack, the success rates of TOG-F on YOLOv5 are close to zero in the case of the universal attack. We also find that the average success rates on BDD100K dataset are higher than MS COCO dataset, since the images in BDD100K are mainly driving scenarios and the features are similar in different images.

Fig. 6 shows the visualization results of the universal perturbations for the target objects (e.g., bird, cat, person and rider). In order to visualize these perturbations more clearly,



Fig. 7. The subjective illustrations of the universal attacks (cat and person) on FasterRCNN and YOLOv5. The first two rows are the detection results of MS COCO dataset while the last two rows are the detection results of BDD100K dataset. Better to zoom in electronic version for viewing.

we normalize the values from $(-16, 16)$ to $(0, 255)$. The first and second rows are the generated universal perturbations using FasterRCNN and YOLOv5 respectively. We can see that the general outlines of these target objects can be recognized in the universal perturbations, which implies the proposed method precisely locates the critical features of the target objects from the guided images. Then, the perturbations are added to different source images to achieve the universal attack. Fig. 7 illustrates some subjective detection results of MS COCO and BDD100K datasets by applying the universal perturbations of cat and person on FasterRCNN and YOLOv5.

3) *Generalization Performance*: In addition to the above image-specific attack and universal attack, we further employ the generated universal perturbations to attack unseen data to evaluate the generalization performance of the proposed method. Specifically, we randomly select other 200 images from each of MS COCO and BDD100K datasets to construct the adversarial examples. It should be noted that these 200 images are not included in the source image set \mathcal{X}^s during

TABLE V
THE GENERALIZATION PERFORMANCE COMPARISONS BETWEEN TOG-F AND THE PROPOSED TFA ON MS COCO DATASET.

Detector	Method	bird	cat	car	cow	dog	laptop	motor	teddy	average
FasterRCNN	TOG-F	29.7	17.6	55.0	28.8	11.5	8.3	11.3	17.6	22.5
	TFA	43.8	54.0	63.9	28.3	43.5	50.3	20.6	36.4	42.6
YOLOv5	TOG-F	1.0	3.7	1.1	0.0	0.0	0.0	0.0	1.0	0.9
	TFA	85.3	69.6	92.6	76.8	78.9	85.2	71.4	70.5	78.8

TABLE VI
THE GENERALIZATION PERFORMANCE COMPARISONS BETWEEN TOG-F AND THE PROPOSED TFA ON BDD100K DATASET.

Detector	Method	bike	bus	motor	person	rider	truck	average
FasterRCNN	TOG-F	64.8	73.9	63.4	81.3	56.4	73.7	68.9
	TFA	99.4	88.6	85.6	99.1	75.2	88.0	89.3
YOLOv5	TOG-F	0.0	2.6	0.0	0.0	0.0	3.8	1.1
	TFA	99.5	96.9	97.9	100.0	92.0	98.1	97.4

the training process.

The attack success rates with regard to the generalization performance are shown in Table V and Table VI. On MS COCO dataset, TFA achieves 42.6 and 78.8 average success rates when attacking FasterRCNN and YOLOv5, while TOG-F only achieves 22.5 and 0.9 average success rates. Similar results occur on BDD100K dataset, TFA achieves 89.3 and 97.4 average success rates while TOG-F only achieves 68.9 and 1.1 average success rates, respectively. These comparisons show that the proposed TFA has a stronger generalization capability than TOG-F.

Besides, we also observe that the success rates of the generalization performance of TFA in Table V and Table VI are comparable to the results in Table I and Table II. This means that the universal perturbations generated by the proposed method do contain the critical semantic information of the target objects and can effectively attack both the training data and unseen data.

C. Detailed Analysis on TFA

1) *Analysis of Perturbation Degree:* In the hyperparameter setting, the restriction value of the adversarial perturbation ϵ is fixed to 16. However, different perturbation degrees have different attack effects for the targeted attack method. Table VII shows the comparison results of TFA when attacking FasterRCNN and YOLOv5 in the cases of $\epsilon=4, 8, 12, 16$ and 20 respectively. We can see that the success rates of TFA attack on FasterRCNN drop significantly as the decrease of ϵ . When ϵ is set to 4, the corresponding success rate is close to zero. In contrast, the proposed method keeps high performance (> 96) for the YOLOv5 attack as long as ϵ is greater than 8. The success rate is 48.3 even if ϵ is set to 4. This comparison demonstrates that FasterRCNN may be more sensitive to the adversarial perturbation and the extracted features of YOLOv5 can be easily changed even with small perturbation.

Fig. 8 illustrates the detection results of TFA at different ϵ . The first and second rows are the visualization results of FasterRCNN and YOLOv5 for one image sample, respectively. The target object is a bird, and it can be observed that TFA successfully misleads YOLOv5 to predict a bird with various

TABLE VII
THE COMPARISON RESULTS OF TFA WHEN ATTACKING FASTERRCNN AND YOLOV5 IN THE CASES OF DIFFERENT ϵ .

Detector	4	8	12	16	20
FasterRCNN	0.8	8.0	26.6	42.1	51.0
YOLOv5	48.3	96.1	99.6	99.8	99.9

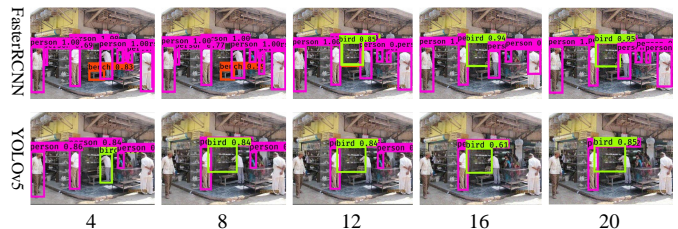


Fig. 8. The visualization results of different perturbation degrees ($\epsilon = 4, 8, 12, 16, 20$). The first and second rows are the detection results of TFA attack on FasterRCNN and YOLOv5 respectively. The target object is a bird.

configurations of ϵ while the attacks on FasterRCNN fail in the cases of $\epsilon=4$ and $\epsilon=8$.

2) *Ablation Study on Dual Attention:* As presented in Section III, the dual attention mechanism is a key component for the proposed TFA because it can filter out the critical features of the target object in the whole feature space. Therefore, we conduct an ablation study to demonstrate the effectiveness of the class attention and the spatial attention. Specifically, the attack success rates of TFA on FasterRCNN and YOLOv5 are evaluated respectively in the cases of $\mathbf{w}_i = 1$, $\mathbf{w}_i = w_i^c$, $\mathbf{w}_i = \mathbf{w}_i^s$ and $\mathbf{w}_i = w_i^c \times \mathbf{w}_i^s$. Table VIII shows the results of the ablation study on MS COCO dataset, where none attention corresponds to $\mathbf{w}_i = 1$, class attention corresponds to $\mathbf{w}_i = w_i^c$, spatial attention corresponds to $\mathbf{w}_i = \mathbf{w}_i^s$, and dual attention corresponds to $\mathbf{w}_i = w_i^c \times \mathbf{w}_i^s$. We note that the results of YOLOv5 is obtained in the cast of $\epsilon=8$ for a clear comparison.

As it can be observed, almost all the attack success rates of the none attention are the lowest because this case optimizes the whole feature space equally and does not focus on the critical features of the target objects. With the use of class attention or spatial attention, the success rate increases to some

TABLE VIII

THE COMPREHENSIVE ABLATION STUDY RESULTS OF THE PROPOSED DUAL ATTENTION MECHANISM ON ATTACKING FASTERRCNN AND YOLOV5.

Detector	Attention	bird	cat	car	cow	dog	laptop	motor	teddy	average
FasterRCNN	None attention	28.5	41.6	30.0	14.4	37.1	36.9	15.2	6.7	26.3
	Class attention	37.6	44.4	35.4	15.4	40.6	42.9	25.0	14.3	32.0
	Spatial attention	31.6	42.2	32.3	19.3	38.4	39.2	18.8	10.5	29.0
	Dual attention	40.4	55.7	35.9	27.2	46.3	50.4	48.7	32.3	42.1
YOLOv5	None attention	94.9	74.9	92.7	98.8	89.0	97.2	92.9	86.9	90.9
	Class attention	95.9	83.6	97.1	99.7	95.7	97.4	94.5	94.1	94.8
	Spatial attention	96.1	79.8	95.3	99.6	96.1	99.0	95.8	90.5	94.0
	Dual attention	96.2	84.2	98.3	99.9	98.3	99.0	96.8	95.7	96.1

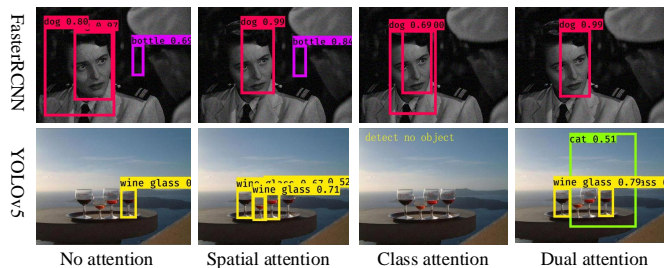


Fig. 9. The subjective illustrations of the ablation study for TFA. The guided images and the target objects (i.e. dog and cat) are shown in Fig. 5.

extent, and the dual attention gains the optimal performance. Fig. 9 illustrates two samples of the corresponding subjective results for TFA. The first row is an example of attacking FasterRCNN with a dog as the target object, we can see that the detector predicts multiple objects other than the dog or predicts wrong positions in the first three columns, while the proposed dual attention ensures that the specific class can be detected uniquely in the right position. The second row is an example of attacking YOLOv5 with a cat as the target object, the detector can not predict the specific cat with only spatial attention or class attention, while the specific class can be fabricated successfully by employing the dual attention mechanism.

3) *Impact of Guided Image*: Guided image is another key component in the proposed TFA method as presented in Section III. In the experimental setting, we randomly selected one sample containing the target object as the guided image. Therefore, it is necessary to evaluate the impacts of different

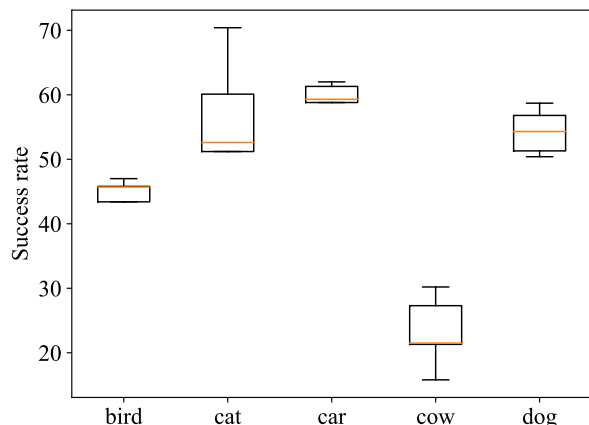


Fig. 10. The success rates of different guided images for attacking FasterRCNN on MS COCO dataset.

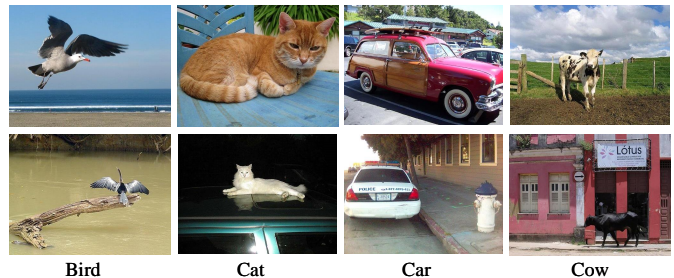


Fig. 11. The subjective illustrations of different guided images. The images in first row achieve highest success rates for corresponding class while the images in second row achieve the lowest success rates.

guided images for one specific class. Fig. 10 illustrates the success rates of different guided images for attacking FasterRCNN on MS COCO dataset. We can observe that different guided images of one specific class have distinctive attack performances. Taking the specific class dog as an example, the success rate varies from 50.4 to 58.7 for different guided images. Fig. 11 shows some guided images associated with the lowest and highest success rates of four target objects. According to the experimental results and our analysis, we argue that the guided image including a complete and clear target object promotes the attack success rate.

The experiments on the impact of guided image show that the proposed TFA could further improve the attack performance if the guided images are assigned carefully rather than random selection. However, the above comparisons have shown the significant improvement of TFA over TOG-F even with the random selection.

D. TA-fabrication Mode vs. TA-mislabeled Mode

In Section I, we claim that the proposed TA-fabrication mode has three advantages than the existing TA-mislabeled mode. Therefore, additional experiments on MS COCO dataset are conducted in this subsection to compare the image-specific attack, universal attack and generalization attack performances between these two modes. We note that TFA and TOG-M are used to implement the TA-fabrication mode and TA-mislabeled mode respectively.

1) *Image-specific Attack*: Table IX shows the image-specific attack success rates of the proposed TA-fabrication mode and the existing TA-mislabeled mode. We can see that the average success rates of the TA-fabrication are 42.1 and 99.8 for attacking FasterRCNN and YOLOv5, while the average success rates of the TA-mislabeled are only 15.3

TABLE IX
THE COMPARISONS OF IMAGE-SPECIFIC ATTACK SUCCESS RATES BETWEEN THE PROPOSED TA-FABRICATION AND TA-MISLABELING FOR ATTACKING FASTERRCNN AND YOLOV5 ON MS COCO DATASET.

Detector	Mode	Method	bird	cat	car	cow	dog	laptop	motor	teddy	average
FasterRCNN	TA-mislabel	TOG-M	15.6	24.2	10.5	8.6	26.9	11.7	6.6	18.1	15.3
	TA-fabrication	TFA	40.4	55.7	35.9	27.2	46.3	50.4	48.7	32.3	42.1
YOLOv5	TA-mislabel	TOG-M	5.9	11.7	3.6	4.0	14.8	4.1	1.7	6.5	6.5
	TA-fabrication	TFA	99.8	98.4	99.9	100.0	100.0	100.0	100.0	99.9	99.8

TABLE X
THE COMPARISONS OF UNIVERSAL PERFORMANCE BETWEEN THE PROPOSED TA-FABRICATION AND TA-MISLABELING FOR ATTACKING FASTERRCNN AND YOLOV5 ON MS COCO DATASET.

Detector	Mode	Method	bird	cat	car	cow	dog	laptop	motor	teddy	average
FasterRCNN	TA-mislabel	TOG-M	0.6	1.2	0.9	0.1	1.7	0.3	0.0	0.1	0.6
	TA-fabrication	TFA	44.3	55.1	57.2	25.8	40.1	49.9	25.0	35.3	41.6
YOLOv5	TA-mislabel	TOG-M	0.0	0.5	0.2	0.0	0.0	0.0	0.0	0.3	0.1
	TA-fabrication	TFA	88.1	77.8	91.7	88.1	84.4	88.0	81.9	80.3	85.0

TABLE XI
THE COMPARISONS OF GENERALIZATION CAPABILITY BETWEEN THE PROPOSED TA-FABRICATION AND TA-MISLABELING FOR ATTACKING FASTERRCNN AND YOLOV5 ON MS COCO DATASET.

Detector	Mode	Method	bird	cat	car	cow	dog	laptop	motor	teddy	average
FasterRCNN	TA-mislabel	TOG-M	0.0	3.0	0.0	0.0	0.0	0.0	0.0	0.0	0.4
	TA-fabrication	TFA	43.8	54.0	63.9	28.3	43.5	50.3	20.6	36.4	42.6
YOLOv5	TA-mislabel	TOG-M	0.0	0.0	0.0	0.0	0.0	0.0	0.0	0.0	0.0
	TA-fabrication	TFA	85.3	69.6	92.6	76.8	78.9	85.2	71.4	70.5	78.8

and 6.5, respectively. In principle, the TA-mislabeling attack depends on the detected objects in the source images and attempts to change their original labels. Hence, it is really difficult to achieve a high success rate if the original label and the specified wrong label are total different. Fig. 12 visualizes the attack success rates of the TA-mislabel mode (MS COCO dataset) when attacking the detected objects in the source images to different kinds of target objects.

As it can be observed, the attack success rates are high if the original objects and the target objects have similar characteristics (e.g. car and bus), while the attack success rates are close to zero if the original objects are misled to completely dissimilar objects, such as attacking a car to a sheep. By

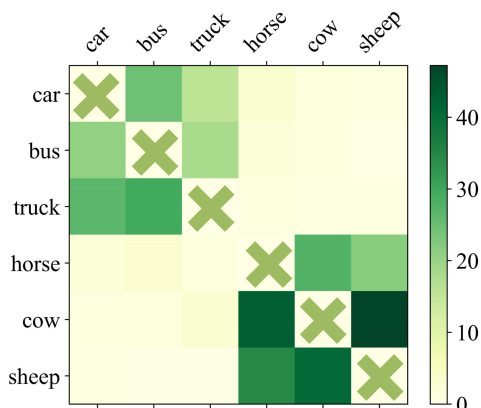


Fig. 12. The attack success rates of the TA-mislabel mode (MS COCO dataset) when attacking the detected objects in source images to different kinds of target objects. The Y-axis represents the existing objects in source images and the X-axis represents the target objects. The diagonal means no attack.

contrast, the proposed TA-fabrication mode can achieve much higher image-specific attack success rates even without similar objects or any detected objects in the source images.

2) *Universal Performance*: The universal performance comparisons between the proposed TA-fabrication and TA-mislabeling are shown in Table X. Obviously, the TA-mislabeling attack has poor universal performance (0.6/0.1) because the detected objects with same class in different source images may have different scales, colors, positions and features.

Compared with the TA-mislabeling, since the adversarial examples generated by the TA-fabrication are independent of the detected objects, the proposed TA-fabrication achieves high universal attack success rates of 41.6/85.0 for attacking FasterRCNN/YOLOv5.

3) *Generalization Capability*: The generalization capability comparisons between the proposed TA-fabrication mode and TA-mislabeling mode are shown in Table XI. As mentioned in subsection IV-B, the universal perturbation generated by TA-fabrication contains the critical semantic information of the target objects, thus it can effectively attack both the training data and unseen data. Therefore, the TA-fabrication mode has strong generalization capability and achieves the success rates of 42.6/78.8 for attacking FasterRCNN/YOLOv5. Compared with the TA-fabrication, the TA-mislabeling has weak generalization capability due to its poor universal performance.

V. CONCLUSION

This work proposes a new targeted attack mode (i.e. TA-fabrication mode) for object detection to mislead detectors

to detect extra false objects with specific target labels. Because the previous methods cannot be directly applied to TA-fabrication mode, we further design a novel attention based feature space attack method (TFA) that drives the extracted features of the source images towards the target objects' features in the guided images, thus achieving the targeted attack of a specific class. Extensive evaluations on multiple datasets (MS COCO and BDD100K) and detectors (Faster-RCNN and YOLOv5) show that the proposed TFA method and TA-fabrication mode have better performances in terms of image-specific attack, universal attack and generalization capability compared with previous works.

REFERENCES

- [1] W. Fang, L. Shen, and Y. Chen, "Survey on image object detection algorithms based on deep learning," in *The International Conference on Artificial Intelligence and Security*, vol. 12736, 2021, pp. 468–480.
- [2] D. Feng, C. Haase-Schütz, L. Rosenbaum, H. Hertlein, C. Gläser, F. Timm, W. Wiesbeck, and K. Dietmayer, "Deep multi-modal object detection and semantic segmentation for autonomous driving: Datasets, methods, and challenges," *IEEE Transactions on Intelligent Transportation Systems*, vol. 22, no. 3, pp. 1341–1360, 2021.
- [3] E. Arnold, O. Y. Al-Jarrah, M. Dianati, S. Fallah, D. Oxtoby, and A. Mouzakitis, "A survey on 3d object detection methods for autonomous driving applications," *The IEEE Transactions on Intelligent Transportation Systems*, vol. 20, no. 10, pp. 3782–3795, 2019.
- [4] P. K. Mishra and G. Saroha, "A study on video surveillance system for object detection and tracking," in *The IEEE International Conference on Computing for Sustainable Global Development*, 2016, pp. 221–226.
- [5] I. S. Kim, H. S. Choi, K. M. Yi, J. Y. Choi, and S. G. Kong, "Intelligent visual surveillance—a survey," *International Journal of Control, Automation and Systems*, vol. 8, no. 5, pp. 926–939, 2010.
- [6] H. Kim, H. Kim, S. Lee, and H. Lee, "Autonomous exploration in a cluttered environment for a mobile robot with 2d-map segmentation and object detection," *IEEE Robotics and Automation Letters*, vol. 7, no. 3, pp. 6343–6350, 2022.
- [7] Z. Li, B. Xu, D. Wu, K. Zhao, M. Lu, and J. Cong, "A mobile robotic arm grasping system with autonomous navigation and object detection," in *The International Conference on Control, Automation and Information Sciences*, 2021, pp. 543–548.
- [8] C. Szegedy, W. Zaremba, I. Sutskever, J. Bruna, D. Erhan, I. Goodfellow, and R. Fergus, "Intriguing properties of neural networks," in *The International Conference on Learning Representations*, 2014, pp. 1–10.
- [9] N. Akhtar, A. Mian, N. Kardan, and M. Shah, "Advances in adversarial attacks and defenses in computer vision: A survey," *IEEE Access*, vol. 9, pp. 155 161–155 196, 2021.
- [10] S. Qiu, Q. Liu, S. Zhou, and C. Wu, "Review of artificial intelligence adversarial attack and defense technologies," *Applied Sciences*, vol. 9, no. 5, p. 909, 2019.
- [11] D. Wang, C. Li, S. Wen, Q. Han, S. Nepal, X. Zhang, and Y. Xiang, "Daedalus: Breaking nonmaximum suppression in object detection via adversarial examples," *IEEE Transactions on Cybernetics*, vol. 52, no. 8, pp. 7427–7440, 2022.
- [12] J. Lu, H. Sibai, and E. Fabry, "Adversarial examples that fool detectors," *CoRR*, vol. abs/1712.02494, 2017.
- [13] Q. Liao, X. Wang, B. Kong, S. Lyu, Y. Yin, Q. Song, and X. Wu, "Category-wise attack: Transferable adversarial examples for anchor free object detection," *CoRR*, vol. abs/2003.04367, 2020.
- [14] Z. Cai, X. Xie, S. Li, M. Yin, C. Song, S. V. Krishnamurthy, A. K. Roy-Chowdhury, and M. S. Asif, "Context-aware transfer attacks for object detection," *CoRR*, vol. abs/2112.03223, 2021.
- [15] O. M. Nezami, A. Chaturvedi, M. Dras, and U. Garain, "Pick-object-attack: Type-specific adversarial attack for object detection," *Computer Vision and Image Understanding*, vol. 211, pp. 1–1, 2021.
- [16] D. Li, J. Zhang, and K. Huang, "Universal adversarial perturbations against object detection," *Pattern Recognition*, vol. 110, pp. 1–12, 2021.
- [17] H. Zhang, W. Zhou, and H. Li, "Contextual adversarial attacks for object detection," in *The IEEE International Conference on Multimedia and Expo*, 2020, pp. 1–6.
- [18] X. Wei, S. Liang, N. Chen, and X. Cao, "Transferable adversarial attacks for image and video object detection," in *The International Joint Conference on Artificial Intelligence*, 2019, pp. 954–960.
- [19] C. Xie, J. Wang, Z. Zhang, Y. Zhou, L. Xie, and A. Yuille, "Adversarial examples for semantic segmentation and object detection," in *The IEEE International Conference on Computer Vision*, 2017, pp. 1369–1378.
- [20] K.-H. Chow, L. Liu, M. Loper, J. Bae, M. E. Gursoy, S. Truex, W. Wei, and Y. Wu, "Adversarial objectness gradient attacks in real-time object detection systems," in *The IEEE International Conference on Trust, Privacy and Security in Intelligent Systems and Applications*, 2020, pp. 263–272.
- [21] Y. Wang, K. Wang, Z. Zhu, and F. Wang, "Adversarial attacks on faster R-CNN object detector," *Neurocomputing*, vol. 382, pp. 87–95, 2020.
- [22] A. Shapira, A. Zolfi, L. Demetrio, B. Biggio, and A. Shabtai, "Denial-of-service attack on object detection model using universal adversarial perturbation," *CoRR*, vol. abs/2205.13618, 2022.
- [23] S. Ren, K. He, R. B. Girshick, and J. Sun, "Faster R-CNN: towards real-time object detection with region proposal networks," in *The Advances in Neural Information Processing Systems*, 2015, pp. 91–99.
- [24] G. Jocher, "ultralytics/yolov5: v6.1 - tensorrt, tensorflow edge tpu and openvino export and inference," 2021. [Online]. Available: <https://zenodo.org/record/6222936#.YsBHQxVByUk>
- [25] I. J. Goodfellow, J. Shlens, and C. Szegedy, "Explaining and harnessing adversarial examples," *arXiv preprint arXiv:1412.6572*, 2014.
- [26] J. Wang, A. Liu, X. Bai, and X. Liu, "Universal adversarial patch attack for automatic checkout using perceptual and attentional bias," *IEEE Transactions on Image Processing*, vol. 31, pp. 598–611, 2022.
- [27] N. Li and Z. Chen, "Toward visual distortion in black-box attacks," *IEEE Transactions on Image Processing*, vol. 30, pp. 6156–6167, 2021.
- [28] Z. Wang, H. Guo, Z. Zhang, W. Liu, Z. Qin, and K. Ren, "Feature importance-aware transferable adversarial attacks," in *The IEEE/CVF International Conference on Computer Vision*, 2021, pp. 7619–7628.
- [29] A. V. Subramanyam, "Sinkhorn adversarial attack and defense," *IEEE Transactions on Image Processing*, vol. 31, pp. 4039–4049, 2022.
- [30] B. Yin, W. Wang, T. Yao, J. Guo, Z. Kong, S. Ding, J. Li, and C. Liu, "Adv-makeup: A new imperceptible and transferable attack on face recognition," in *The International Joint Conference on Artificial Intelligence*, 2021, pp. 1252–1258.
- [31] J. Sun, Y. Cao, Q. A. Chen, and Z. M. Mao, "Towards robust lidar-based perception in autonomous driving: General black-box adversarial sensor attack and countermeasures," in *USENIX Security Symposium*, S. Capkun and F. Roesner, Eds., 2020, pp. 877–894.
- [32] J. Tu, M. Ren, S. Manivasagam, M. Liang, B. Yang, R. Du, F. Cheng, and R. Urtasun, "Physically realizable adversarial examples for lidar object detection," pp. 13 713–13 722, 2020.
- [33] S. Jia, Y. Song, C. Ma, and X. Yang, "Iou attack: Towards temporally coherent black-box adversarial attack for visual object tracking," in *The IEEE Conference on Computer Vision and Pattern Recognition*, 2021, pp. 6709–6718.
- [34] L. Wang and K.-J. Yoon, "PSAT-GAN: efficient adversarial attacks against holistic scene understanding," *IEEE Transactions on Image Processing*, vol. 30, pp. 7541–7553, 2021.
- [35] L. Zhao, C. Chen, and J. Huang, "Deep learning-based forgery attack on document images," *IEEE*.
- [36] R. R. Selvaraju, M. Cogswell, A. Das, R. Vedantam, D. Parikh, and D. Batra, "Grad-CAM: Visual explanations from deep networks via gradient-based localization," in *The IEEE International Conference on Computer Vision*, 2017, pp. 618–626.
- [37] B. Zhou, A. Khosla, A. Lapedriza, A. Oliva, and A. Torralba, "Object detectors emerge in deep scene CNNs," in *The International Conference on Learning Representations*, 2015, pp. 1–12.
- [38] J. Fu, J. Liu, H. Tian, Y. Li, Y. Bao, Z. Fang, and H. Lu, "Dual attention network for scene segmentation," in *The IEEE Conference on Computer Vision and Pattern Recognition*, 2019, pp. 3146–3154.
- [39] C. Zhang, P. Benz, T. Imtiaz, and I. S. Kweon, "Understanding adversarial examples from the mutual influence of images and perturbations," in *The IEEE/CVF Conference on Computer Vision and Pattern Recognition*, 2020.
- [40] L. Gao, Y. Cheng, Q. Zhang, X. Xu, and J. Song, "Feature space targeted attacks by statistic alignment," in *The International Joint Conference on Artificial Intelligence*, 2021, pp. 671–677.
- [41] K. R. Mopuri, A. Ganeshan, and R. V. Babu, "Generalizable data-free objective for crafting universal adversarial perturbations," *The IEEE Transactions on Pattern Analysis and Machine Intelligence*, vol. 41, no. 10, pp. 2452–2465, 2019.
- [42] D. Li, J. Zhang, and K. Huang, "Universal adversarial perturbations against object detection," *Pattern Recognition*, vol. 110, p. 107584, 2021.
- [43] T. Lin, M. Maire, S. J. Belongie, J. Hays, P. Perona, D. Ramanan, P. Dollár, and C. L. Zitnick, "Microsoft COCO: common objects in

- context,” in *The European Conference on Computer Vision*, 2014, pp. 740–755.
- [44] F. Yu, H. Chen, X. Wang, W. Xian, Y. Chen, F. Liu, V. Madhavan, and T. Darrell, “BDD100K: A diverse driving dataset for heterogeneous multitask learning,” in *The IEEE/CVF Conference on Computer Vision and Pattern Recognition*, 2020, pp. 2633–2642.
- [45] A. Mahendran and A. Vedaldi, “Understanding deep image representations by inverting them,” in *The IEEE Conference on Computer Vision and Pattern Recognition*, 2015, pp. 5188–5196.